Journal of Materials Chemistry A

RSCPublishing

Paper

Sodium-Ion Battery Cathodes $Na_2FeP_2O_7$ and $Na_2MnP_2O_7$: Diffusion Behaviour for High Rate Performance

Cite this: DOI: 10.1039/xoxxoooooox

Received ooth January 2012,
Accepted ooth January 2012

DOI: 10.1039/xoxxoooooox

www.rsc.org/

John M. Clark,[a] Prabeer Barpanda,[b,c,d] Atsuo Yamada,[b,d] and M. Saiful Islam[a*]

Na-ion batteries are currently the focus of significant research interest due to the relative abundance of sodium and its consequent cost advantages. Recently, the pyrophosphate family of cathodes has attracted considerable attention, particularly $Li_2FeP_2O_7$ due to its high operating voltage and enhanced safety properties; in addition the sodium-based pyrophosphates $Na_2FeP_2O_7$ and $Na_2MnP_2O_7$ are also generating interest. Herein, we present defect chemistry and ion migration results, determined via atomistic simulation techniques, for $Na_2MP_2O_7$ (where M = Fe, Mn) as well as findings for $Li_2FeP_2O_7$ for direct comparison. Within the pyrophosphate framework the most favourable intrinsic defect type is found to be the antisite defect, in which alkali-cations (Na/Li) and M ions exchange positions. Low activation energies are found for long-range diffusion in all crystallographic directions in $Na_2MP_2O_7$ suggesting three-dimensional (3D) Na-ion diffusion. In contrast $Li_2FeP_2O_7$ supports 2D Li-ion diffusion. The 2D or 3D nature of the alkali-ion migration pathways within these pyrophosphate materials means that antisite defects are much less likely to impede their transport properties, and hence important for high rate performance.

1. Introduction

Li-ion batteries have dominated the portable energy storage market during the past two decades[1-7] due to their lightweight, high energy density and high power, which all depend critically on fast Li-ion mobility. Despite the wide-spread use of Li-ion cells, batteries based on alternative carrier ions such as sodium ions could be more suitable for large-scale energy storage systems. Whilst the higher gravimetric capacity afforded by Li-ion cells is critical for portable applications, the relative abundance and low cost associated with Na-ion batteries now make them an attractive alternative for grid storage.[8,9]

Substantial research effort has been invested during the previous decades to produce electrode materials for sodium batteries that will allow for facile intercalation of Na-ions at suitable potentials. Amongst the cathode materials investigated, a variety of layered oxides (e.g. $NaxCO_2$, $NaCrO_2$, $NaVO_2$, $Na_x[Fe_{0.5}Mn_{0.5}]O_2$) and polyanionic compounds (e.g. $NaFePO_4$, $Na_3V_2(PO_4)_3$, Na_2FePO_4F, $NaFeSO_4F$) have been reported[10-17].

Recently lithium pyrophosphate-based materials including $Li_2FeP_2O_7$ and $Li_2Fe_xMn_{1-x}P_2O_7$ ($0 \leq x \leq 1$) have been examined,[18-20] which show good electrochemical and thermal properties. It was found that $Li_2FeP_2O_7$ exhibited a redox-potential of 3.5 V vs Li/Li^+ while showing a reversible capacity of ~105 mA h g^{-1},[18] whilst for the mixed-metal pyrophosphate it was found that the partial substitution with Mn was observed to increase the Fe^{3+}/Fe^{2+} redox potential.[19] This pyrophosphate structure can offer partial upshift of the Fe^{3+}/Fe^{2+} redox potential approaching 4 V (vs Li/Li^+) independent of cationic size and redox activity of 3d metal substituants.[21,22] In addition to this high-voltage redox tunability, it is expected that the framework provided by the pyrophosphate anion will give rise to cathode materials with enhanced thermal stabilities.[23]

Motivated by the significance of Na-ion batteries for large-scale storage systems in addition to the promising properties of $Li_2FeP_2O_7$, attempts were made to synthesise a sodium version of the Fe-based pyrophosphate ($Na_2FeP_2O_7$),[24-26] as well as other Na-analogues with different transition-metal active redox species such as a new Mn-based polymorph, β-$Na_2MnP_2O_7$.[27,28] Yamada *et al.*[24] were able to prepare $Na_2FeP_2O_7$ via a conventional one-step solid-state synthesis, and found it to be electrochemically active, delivering a reversible capacity of 82 mA h g^{-1} with an operating voltage around 3 V (vs Na/Na^+). The combination of low cost materials, moderate theoretical capacity (~100 mA h g^{-1}), high rate kinetics and good thermal stability makes $Na_2FeP_2O_7$ a highly promising Na-ion battery material. From a crystal structure view-point, the change of alkali ions from Li to Na results in different crystal frameworks: while $Li_2FeP_2O_7$ adopts the monoclinic ($P2_1/c$) structure[18], $Na_2FeP_2O_7$ adopts the triclinic (P-1) structure[25].

Recently β-$Na_2MnP_2O_7$[27] has also been proposed as a new pyrophosphate cathode for sodium-ion batteries, and found to offer similar (if not slightly superior) electrochemical

performance to $Na_2FeP_2O_7$. $Na_2MnP_2O_7$ exhibits a discharge capacity close to 80 mA h g^{-1} (at 25 ºC) with a voltage of 3.6 V, the highest Mn^{3+}/Mn^{2+} redox potential amongst all Mn-based cathodes. The electrochemical activity of the Mn-containing cathode material is noteworthy, when compared to the Li counterpart ($Li_2MnP_2O_7$), which is almost inactive at room temperature owing to its sluggish kinetics.[28] The β-$Na_2MnP_2O_7$ polymorph crystallises in the triclinic ($P1$) space group[27], isostructural to the rose-polymorph of $Na_2CoP_2O_7$.[29]

The present study uses advanced simulation techniques to investigate important atomic-scale issues related to point defects and alkali (Na/Li) ion migration in $Na_2MP_2O_7$ (M = Fe, Mn,) and $Li_2FeP_2O_7$. The present work extends our previous simulation studies of lithium battery electrodes[30-39] such as $LiMPO_4$ (M = Mn, Fe, Co, Ni),[31-34] and our investigations of sodium-based cathodes such as $NaFeSO_4F$[36] and Na_2FePO_4F.[40]

2. Simulation Methods

This investigation uses well established simulation techniques based on the Born model of solids. As these techniques are described in detail elsewhere[41,42], only a general outline will be given here. All systems were treated as crystalline solids, with interactions between ions consisting of a long-range Coulombic component and a short-range component representing electron-electron repulsion and van der Waals interactions. The short-range interactions were modelled using the Buckingham potential,[41] and the well-known shell model[43] was employed to account for the polarizability effects. As argued previously, interatomic potential methods are assessed primarily by their ability to reproduce observed crystal properties. Indeed, they are found to work well, even for phosphate and silicate cathodes[31-36,39] where there is undoubtedly a degree of covalency. The Fe–O, Mn–O, P–O and O–O interatomic potentials were taken directly from the study of the related $Li_2FeP_2O_7$[39] (to which we compare our defect and migration results), whilst the Na–O potential was taken from the recent study of the Na_2FePO_4F[40] cathode material. The resulting potential parameters are listed in Table S1 (supporting information).

The inclusion of lattice relaxation about defects (such as Na vacancies) and migrating ions was simulated via an implementation of the Mott-Littleton scheme incorporated within GULP (v4.0)[44]. This methodology considers the crystal lattice as two separate regions, with explicit relaxation of the ions in the inner region immediately surrounding the defect (~1000 ions). In contrast, the remainder of the crystal (~3000 ions), where the defect forces are relatively weak, is treated by more approximate quasi-continuum methods.

3. Results and Discussion

3.1 Structural Modelling and Intrinsic Defects

Reproduction of the experimentally observed crystal structures (Figure 1) provided the starting point for the current study. The structure exhibited by $Na_2FeP_2O_7$ is triclinic (P-1),[25] comprised of corner-sharing FeO_6 octahedra creating Fe_2O_{11} dimers, which are interconnected by both corner-sharing and edge-sharing with P_2O_7 pyrophosphate groups. The FeO_6 octahedra and PO_4 tetrahedra are connected in a staggered fashion thus creating large tunnels along the [011] direction within which the Na atoms are present. The Na ions occupy six distinct crystallographic sites; three of which are fully occupied (Na1, Na2, Na3), whilst the other three adopt sites that are partially occupied (Na4, Na5, Na6). To account for the partial occupancy it was necessary to employ a 3×1×1 supercell approach considering different cation ordering schemes as used in previous simulations.[33,36,39] The energetics of the different cation configurations were investigated through a series of geometry optimizations performed under $P1$ symmetry. We note that the lattice energy differences were found to be very small (< 15 meV), suggesting that any ordering of the Na4, Na5 and Na6 sites may not be significant.

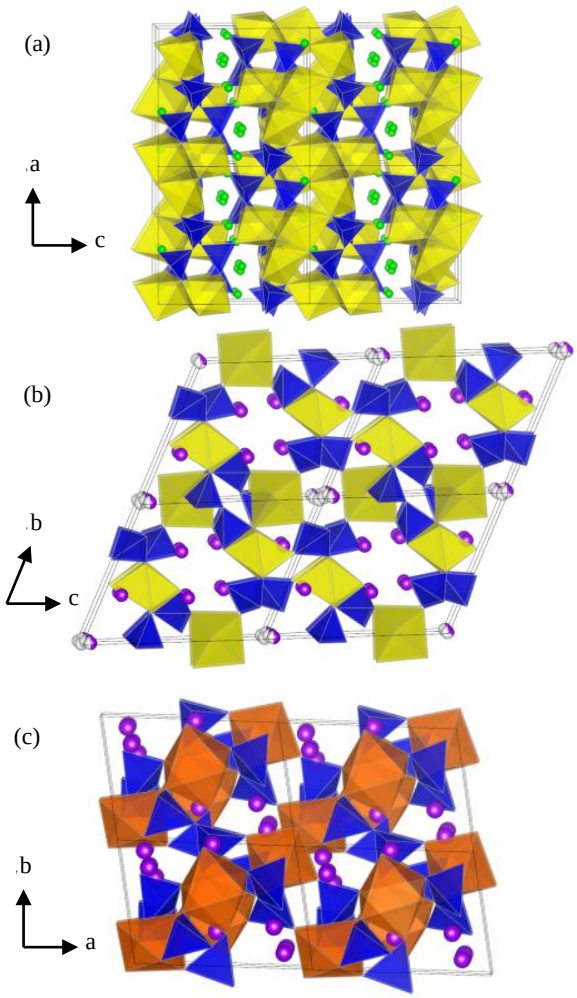

Fig. 1 Crystal structure of $Li_2FeP_2O_7$ and $Na_2MP_2O_7$ (M = Fe, Mn). a.) $Li_2FeP_2O_7$ ($P2_1/c$; c-axis view), b.) $Na_2FeP_2O_7$ (P-1; a-axis view), c.) $Na_2MnP_2O_7$ ($P1$; c-axis view); showing Li ions (green) Na ions (purple), FeO_6 octahedra (yellow), MnO_6 octahedra (orange) and P_2O_7 pyrophosphate units (blue).

The structure exhibited by $Na_2MnP_2O_7$[27] consists of distorted MnO_6 octahedral and tetrahedral building blocks which are connected in a staggered manner thus creating tunnels along the [001] direction. The structures have corner-sharing isolated Mn_2O_{11} dimers, which are in turn connected by the P_2O_7 units by a mixed edge and corner-sharing fashion. The constituent Na atoms are located in eight inequivalent crystallographic sites. It has been postulated that the complex nature of this triclinic ($P1$) structure may allow for multidimensional Na^+ diffusion.[24] Comparisons between the

calculated and experimental crystal structures are given in Table 1.

Table 1 Calculated and Experimental Structural Parameters of $Na_2MP_2O_7$ (*M* = Fe, Mn) and $Li_2FeP_2O_7$.

Param	*a* (Å)	*b* (Å)	*c* (Å)	*α* (°)	*β* (°)	*γ* (°)
			$Na_2FeP_2O_7$			
calc.	6.449	9.483	10.993	64.85	86.24	73.13
expt.[25]	6.433	9.458	11.143	65.16	85.49	73.49
Δ (±)	0.016	0.025	0.150	0.31	0.75	0.36
			$Na_2MnP_2O_7$			
calc.	9.917	11.169	12.489	148.77	121.26	69.00
expt.[27]	9.922	11.084	12.473	148.39	121.95	68.42
Δ (±)	0.005	0.085	0.017	0.38	0.68	0.58
			$Li_2FeP_2O_7$[39]			
calc.	11.017	9.754	9.805	90.00	101.54	90.00
expt.	11.200	9.715	9.791	90.00	102.85	90.00
Δ (±)	0.183	0.039	0.014	0.00	1.31	0.00

For all pyrophosphate systems, the calculated unit cell parameters deviate from experiment by at most 0.18 Å, and in most cases much less; the same is found for the individual bond lengths. The excellent reproduction of the complex low symmetry monoclinic ($Li_2FeP_2O_7$) and triclinic ($Na_2MP_2O_7$) crystal structures gives us confidence that the interatomic potential models can be used reliably in the defect and migration calculations.

Investigation of the defect properties of cathode materials is essential in order to gain a full understanding of their electrochemical behaviour, particularly the possibility of "blocking" antisite defects in structures showing 1D ion conduction. A series of isolated point defect (vacancy and interstitial) energies were calculated for both $Li_2FeP_2O_7$ and $Na_2MP_2O_7$ (*M* = Fe, Mn). By combining these energies, the relative energies of formation of Frenkel and Schottky type defects were determined. These take the following general forms (using Kröger-Vink notation and where *A* = Li, Na):

A Frenkel: $A_A^X \rightarrow V_A' + A_i^\bullet$ (1)

M Frenkel $M_M^X \rightarrow V_M'' + M_i^{\bullet\bullet}$ (2)

O Frenkel $O_O^X \rightarrow V_O^{\bullet\bullet} + O_i''$ (3)

Full Schottky $2A_A^X + M_M^X + 2P_P^X + 7O_O^X \rightarrow 2V_A' + V_M'' + 2V_P'''' + 7V_O^{\bullet\bullet} + A_2MP_2O_7$ (4)

Calculation of the *M*/*A* "antisite" pair defect, involving the exchange of an A^+ ion (Li^+ radius 0.76 Å, Na^+ radius 1.02 Å) with an M^{2+} ion (Fe^{2+} radius 0.78 Å and Mn^{2+} radius 0.83 Å)[45], was considered according to:

M/*A* Antisite $M_M^X + A_A^X \rightarrow A_M' + M_A^\bullet$ (5)

Analysis of the resulting defect energies listed in Table 2 reveals three main points. First, the magnitude of the calculated energies for *M* Frenkel, O Frenkel and Schottky defects suggests their formation is unfavourable. Further to which, it is found that O^{2-} vacancies and interstitials are particularly unfavourable, and highly unlikely to occur in any significant concentration in these undoped materials, thus confirming the structural stability of the pyrophosphate framework in accord with thermal stability experiments[25].

Table 2 Energies of Intrinsic Atomic Defect Processes in $Na_2MP_2O_7$ (*M* = Fe, Mn) and $Li_2FeP_2O_7$.

		Energy (eV)		
Disorder Type	eq.	$Na_2FeP_2O_7$	$Na_2MnP_2O_7$	$Li_2FeP_2O_7$[39]
Li or Na Frenkel	(1)	1.14	1.34	1.21
M Frenkel	(2)	3.52	2.93	3.39
O Frenkel	(3)	3.53	3.92	3.99
Full Schottky	(4)	33.03	38.62	32.42
A/*M* antisite	(5)	0.89	0.80	0.22

Second, the intrinsic defect type found to be most favourable for the $Na_2MP_2O_7$ material is the Na/*M* antisite pair as was predicted for the Li/Fe antisite pair in the analogous study of the Li analogue ($Li_2FeP_2O_7$)[39]. The formation energy for the Na/*M* antisite within the $Na_2MP_2O_7$ materials is of greater magnitude, suggesting lower but still significant concentrations of antisite defects within $Na_2MP_2O_7$. Since Na^+ is significantly larger than Li^+, Fe^{2+} and Mn^{2+} [45], it is perhaps intuitive that Na/*M* antisite defect will be less prominent within the pyrophosphate framework than the analogous Li/Fe antisite as revealed by the calculations. Overall our expectation for such defects is that their concentration of antisite disorder would be temperature dependent and therefore sensitive to the experimental conditions imposed during synthesis.

Lastly, the second lowest energies found for the $Na_2MP_2O_7$ cathode materials were for the Na Frenkel defect formation (Table 2). This result is in accordance with the value calculated for the Li Frenkel defect within $Li_2FeP_2O_7$[39]. This suggests that a very minor population of such Li/Na vacancy and interstitial defects could be present at high temperatures. It should be noted that in terms of ion diffusion, the antisite defects will have greater significance within the olivine materials since their presence will block the only available channel for 1D alkali ion migration.[31,40]

3.2 Na Ion Migration

Examination of the Na^+ mobility and pathways in $Na_2MP_2O_7$ is of vital importance when considering their respective charge/discharge rates and any differences with Li^+ mobility.

Na-diffusion pathways were considered between all neighbouring Na positions within the $Na_2MP_2O_7$ (*M* = Fe, Mn) materials along each of the three principal axes via conventional vacancy hopping. Energy profiles for Na migration along each of the pathways considered can be mapped out, and the migration energies derived; such an approach has been used in numerous previous studies on oxide ion and cation migration in complex oxides.[31,32,46] The resulting lowest migration energies for Na diffusion along the three principal axes of the $Na_2MP_2O_7$ materials are reported in Table 3 with the corresponding lowest migration energies for Li diffusion within $Li_2FeP_2O_7$ reported for comparison[39].

From the results presented in Table 3, it would appear that that both $Na_2MP_2O_7$ structures support quasi-three dimensional (3D) Na^+ diffusion with activation energies of 0.49 eV and 0.58 eV for $Na_2FeP_2O_7$, and $Na_2MnP_2O_7$ respectively. The final calculated paths for long-range Na^+ diffusion are shown in Figures 2 and 3. The $Li_2FeP_2O_7$ compound shows 2D Li^+ diffusion in the bc-plane with an activation energy of 0.40 eV.[39] Therefore in all cases the pyrophosphate framework appears to show high alkali-ion (Na^+/Li^+) mobility. Although

there are no Li^+/Na^+ conductivity data for direct comparison, our calculated values for alkali-ion migration are consistent with experimental activation energies for Li/Na ion conductivity in other framework-structured phosphate materials.[47-49] We note that in a recent theoretical study of a different $Na_2FeP_2O_7$ polymorph (triclinic, P1) Na^+ diffusion was found to be 2D with migration barriers of ~0.54 eV.[26]

Table 3 Calculated Migration Energies for Most Favourable Paths of Alkali-ion Diffusion: Na-ion Migration in $Na_2FeP_2O_7$ and $Na_2MnP_2O_7$ and Li-ion Migration in $Li_2FeP_2O_7$.

Net Diffusion Direction	Migration Energies (eV)		
	$Na_2FeP_2O_7$	$Na_2MnP_2O_7$	$Li_2FeP_2O_7$[39]
a-axis	0.33	0.58	0.73
b-axis	0.42	0.58	0.40
c-axis	0.49	0.58	0.40

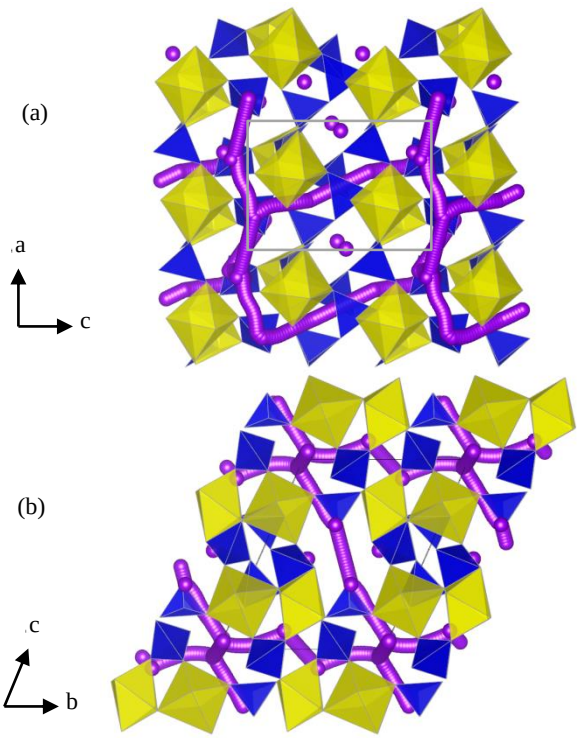

Fig. 2 Calculated paths for long-range Na^+ migration within $Na_2FeP_2O_7$ along the *a*-axis, *b*-axis and *c*-axis directions with activation energies ≤ 0.49 eV; a) view of the *ac*-plane; b) view of the *bc*-plane.

The 2D and 3D transport behaviour in the pyrophosphates contrasts with that in olivine $LiFePO_4$ and $NaFePO_4$ which only allow Li^+/Na^+ migration along 1D channels parallel to the *b*-axis[31,40]. In addition, ion blocking by antisite defects is much less likely to make a significant difference to the alkali (Na/Li) ion migration in these pyrophosphate materials. Electrochemical studies indicate that $Na_2FeP_2O_7$ has excellent rate kinetics, superior to that of $Li_2FeP_2O_7$[39]; this may be related to the high dimensionality (3D) and low migration energy for Na-ion diffusion in $Na_2FeP_2O_7$.

Our simulations also reveal curved paths between adjacent Na/Li sites within each of the pyrophosphate materials studied (Figures 2 and 3). It is worth noting that analogous, curved migration pathways were first predicted for Li^+ diffusion within $LiFePO_4$ based on atomistic calculations,[31] which were subsequently confirmed by neutron diffraction maximum entropy method (MEM) analysis.[50]

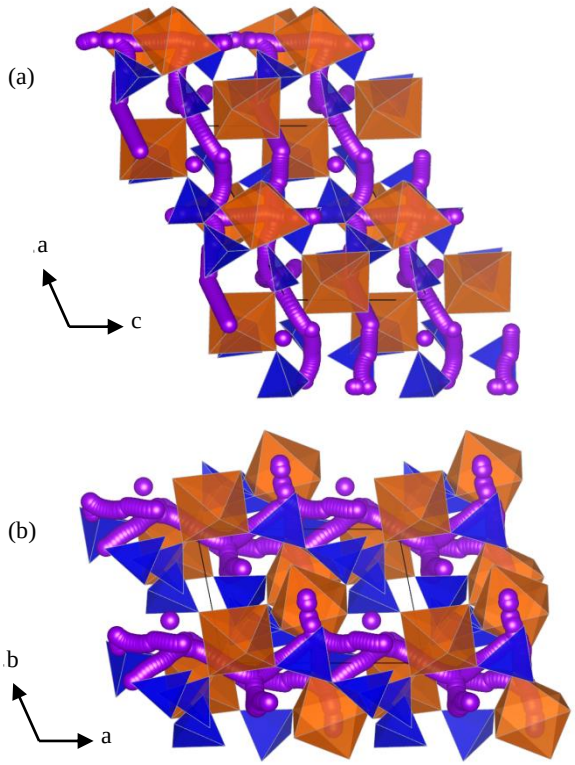

Fig. 3 Calculated paths for long-range Na^+ migration within $Na_2MnP_2O_7$ along the *a*-axis, *b*-axis and *c*-axis directions with activation energies ≤ 0.58 eV; a) view of the *ac*-plane; b) view of the *ab*-plane.

There has been recent debate about the volume difference between the reduced and oxidized phases as a significant factor in determining electrochemical performance of cathode materials.[40,51,52] For two-phase processes, a phase boundary between oxidized and reduced phases is formed during charge/discharge. Electrochemical performance could be affected by the amount of strain generated in this phase boundary, as well as by the activation energy barrier for Li-ion or Na-ion transport.

The difference in the unit cell volume (ΔV) of the oxidized and reduced phases is only ~3.26 % for $Na_2FeP_2O_7$, but > 15 % for $NaFePO_4$ and $NaFeSO_4F$. We note that while the majority of the compounds undergo volume contraction on Li/Na extraction, $Li_2FeP_2O_7$ shows a small volume expansion, although de(lithiation) has been found to be via a solid-solution mechanism in this pyrophosphate[52]. Although the interplay of all factors is still under investigation, materials with a large volume difference between the end member phases could lead to poor rate capability as discussed by Tripathi et al[40]. In contrast, promising electrochemical properties can be anticipated for Na-based cathode materials with low volume change on cycling (e.g. < 7 %) and low ion migration activation barriers (e.g. < 0.5 eV) as in the case of $Na_2FeP_2O_7$ and Na_2FePO_4F.

4. Conclusions

We have investigated Fe- and Mn- based pyrophosphate materials which offer promising high rate cathodes that are potentially low cost and thermally stable for sodium-ion batteries. This survey of $Na_2MP_2O_7$ (M = Fe, Mn) with comparison to $Li_2FeP_2O_7$ used atomistic simulation techniques to provide insights into their defect and ion migration properties.

First, the simulations show good reproduction of the observed complex structures of $Na_2FeP_2O_7$ and $Na_2MnP_2O_7$. The defect calculations indicate the stability of the pyrophosphate framework towards oxygen evolution, which is important for operational safety. The most favourable intrinsic defect type is the Na/M and Li/Fe antisite, with the relative energies suggesting greater Li/Fe disorder in the $Li_2FeP_2O_7$ material as observed.

Secondly, both $Na_2FeP_2O_7$ and $Na_2MnP_2O_7$ are predicted to exhibit curved diffusion pathways parallel to the *a*-, *b*- and *c*-axes with low migration energies (~0.50 eV). Hence, the pyrophosphate framework appears to support 3D Na^+ diffusion in $Na_2MP_2O_7$, (and 2D Li^+ diffusion in $Li_2FeP_2O_7$), which is consistent with the high rate kinetics observed for $Na_2FeP_2O_7$.

Acknowledgements

This work was funded by the EPSRC Supergen programme and made use of the high-performance computing service HECToR, via the HPC Materials Chemistry Consortium. PB thanks the Japan Society for the Promotion of Sciences for a JSPS Fellowship. VESTA[53] was used for analysis of results.

Notes and references

[a] Department of Chemistry, University of Bath, Bath, BA2 7AY, United Kingdom.

[b] Department of Chemical System Engineering, School of Engineering, The University of Tokyo, 7-3-1 Hongo, Bunkyo-Ku, Tokyo 113-8656, Japan.

[c] Materials Research Center, Indian Institute of Science, Bangalore 560012, India.

[d] Unit of Element Strategy Initiative for Catalysts & Batteries, ESICB, Kyoto University, Kyoto 615-8510, Japan.

† Electronic Supplementary Information (ESI) available: [details of any supplementary information available should be included here]. See DOI: 10.1039/b000000x/

1. M. Armand, J. M. Tarascon, *Nature* **2008**, 451, 652.
2. J. B. Goodenough, Y. Kim, *Chem. Mater.* **2010**, 22, 587.
3. B. L. Ellis, K. T. Lee, L. F. Nazar, *Chem. Mater.* **2010**, 22, 691.
4. M. R. Palacin, *Chem. Soc. Rev.* **2009**, 38, 2565.
5. C. Masquelier, L. Croguennec *Chem. Rev.* **2013**, 113, 6552.
6. V. Etacheri, R. Marom, R. Elazari, G. Salitra, D. Aurbach, *Energy Environ. Sci.* **2011,** 4, 3243.
7. Z. L. Gong, Y. Yang, *Energy Environ. Sci.* **2011,** 4, 3223.
8. B. L. Ellis, L. F. Nazar, *Curr. Opin. Solid State Mater. Sci.* **2012**, 16, 168.
9. V. Palomares, P. Serras, I. Villaluenga, K. B. Hueso, J. Carretero-Gonzalez, T. Rojo, *Energy Environ. Sci.* **2012**, *5*, 5884.
10. C. Delmas, J. J. Braconnier, C. Fouassier, P. Hagenmuller, *Solid State Ionics* **1981**, *4*, 165.
11. S. Komaba, C. Takei, T. Nakayama, A. Ogata, N. Yabuuchi, *Electrochem. Commun.* **2010**, *12*, 355.
12. N. Yabuuchi, M. Kajiyama, J. Iwatate, H. Nishikawa, S. Hitomi, R. Okuyama, R. Usui, Y. Yamada, S. Komaba, *Nat. Mater.* **2012**, *11*, 512.
13. P. Moreau, D. Guyomard, J. Gaubicher, F. Boucher, *Chem. Mater.* **2010**, *22*, 4126.
14. Z. L. Jian, L. Zhao, H. L. Pan, Y. S. Hu, H. Li, W. Chen, L. Q. Chen, *Electrochem. Commun.* **2012**, *14*, 86.
15. J. Barker, M. Y. Saidi, J. L. Swoyer, *Electrochem. Solid State Lett.* **2003**, *6*, A1.
16. B. L. Ellis, W. R. M. Makahnouk, Y. Makimura, K. Toghill, L. F. Nazar, *Nat. Mater.* **2007**, *6*, 749.
17. P. Barpanda, J. N. Chotard, N. Recham, C. Delacourt, M. Ati, L. Dupont, M. Armand, J. M. Tarascon, *Inorg. Chem.* **2010**, *49*, 7401.
18. S. Nishimura, M. Nakamura, R. Natsui, A. Yamada, *J. Am. Chem. Soc.* **2010**, *132*, 13596.
19. N. Furuta, S. Nishimura, P. Barpanda, A. Yamada, *Chem. Mater.* **2012**, *24*, 1055.
20. M. Tamaru, P. Barpanda, Y. Yamada, S. Nishimura, A. Yamada, *J. Mater. Chem.* **2012**, *22*, 24526.
21. T. Ye, P. Barpanda, S. Nishimura, N. Furuta, S. C. Chung, A. Yamada, *Chem. Mater.* **2013**, *25*, 3623.
22. P. Barpanda, M. Ati, B. C. Melot, G. Rousse, J. N. Chotard, M. L. Doublet, M. T. Sougrati, S. A. Corr, J. C. Jumas, J. M. Tarascon, *Nat. Mater.* **2011**, *10*, 772.
23. M. Tamaru, S. C. Chung, D. Shimizu, S. Nishimura, A. Yamada, *Chem. Mater.* **2013**, *25*, 2538.
24. P. Barpanda, T. Ye, S. Nishimura, S. C. Chung, Y. Yamada, M. Okubo, H. S. Zhou, A. Yamada, *Electrochem. Commun.* **2012**, *24*, 116.
25. P. Barpanda, G. Liu, C. D. Ling, M. Tamaru, M. Avdeev, S. C. Chung, Y. Yamada, A. Yamada, *Chem. Mater.* **2013**, *25*, 3480.
26. H. Kim, R. A. Shakoor, C. Park, S. Y. Lim, J. S. Kim, Y. N. Jo, W. Cho, K. Miyasaka, R. Kahraman, Y. Jung, W. J. Choi, *Adv. Funct. Mater.* **2013**, *23*, 1147.
27. P. Barpanda, T. Ye, M. Avdeev, S. C. Chung, A. Yamada, *J. Mater. Chem. A* **2013**, *1*, 4194.
28. C. S. Park, H. Kim, R. A. Shakoor, E. Yang, S. Y. Lim, R. Kahraman, Y. Jung, W. J. Choi, *J. Am. Chem. Soc.* **2013**, *135*, 2787.
29. F. Erragh, A. Boukhari, E. Elouadi, E. M. Holt, *J. Crystallogr. Spectrosc. Res.* **1991**, *21*, 321.
30. C. Eames, A. R. Armstrong, P. G. Bruce, M. S. Islam, *Chem. Mater.* **2012**, *24*, 2155.
31. M. S. Islam, D. J. Driscoll, C. A. J. Fisher, P. R. Slater, *Chem. Mater.* **2005**, *17*, 5085.
32. C. A. J. Fisher, V. M. H. Prieto, M. S. Islam, M. S. *Chem. Mater.* **2008**, *20*, 5907.
33. G. R. Gardiner, M. S. Islam, *Chem. Mater.* **2010**, *22*, 1242.
34. C. A. J. Fisher, M. S. Islam, *J. Mater. Chem.* **2008**, *18*, 1209.
35. A. R. Armstrong, N. Kuganathan, M. S. Islam, P. G. Bruce, *J. Am. Chem. Soc.* **2011**, *133*, 13031.
36. R. Tripathi, G. R. Gardiner, M. S. Islam, L. F. Nazar, *Chem. Mater.* **2011**, *23*, 2278.
37. N. Kuganathan, M. S. Islam, *Chem. Mater.* **2009**, *21*, 5196.
38. A. R. Armstrong, C. Lyness, P. M. Panchmatia, M. S. Islam, P. G. Bruce, *Nat. Mater.* **2011**, *10*, 223.
39. J. M. Clark, S. Nishimura, A. Yamada, M. S. Islam, *Angew. Chem. Int. Ed.* **2012**, *51*, 13149.
40. R. Tripathi, S. M. Wood, M. S. Islam, L. F. Nazar, *Energy Environ. Sci.* **2013**, *6*, 2257.
41. A. Walsh, A. A. Sokol, C. R. A. Catlow, *Computational Approaches to Energy Materials*. In Wiley-Blackwell, **2013**.
42. M. S. Islam, C. A. J. Fisher, *Chem. Soc. Rev.* **2014**, 43, 185.
43. B. G. Dick, A. W. Overhauser, *Phys. Rev.* **1958**, *112*, 90.
44. J. D. Gale, A. L. Rohl, *Mol. Simul.* **2003**, *29*, 291.
45. R. D. Shannon, *Acta Crystallogr.* **1976**, *A32*, 751.
46. M. S. Islam, P. R. Slater, *MRS Bull.* **2009**, *34*, 935.
47. C. Delacourt, L. Laffont, R. Bouchet, C. Wurm, J. B. Leriche, M. Morcrette, J. M. Tarascon, C. Masquelier, *J. Electrochem. Soc.* **2005**, *152*, A913.
48. J. Y. Li, W. L. Yao, S. Martin, D. Vaknin, *Solid State Ionics* **2008**, *179*, 2016.
49. L. Sebastian, J. Gopalakrishnan, *J. Mater. Chem.* **2003**, *13*, 433.
50. S. Nishimura, G. Kobayashi, K. Ohoyama, R. Kanno, M. Yashima, A. Yamada, *Nat. Mater.* **2008**, *7*, 707.
51. Y. Zhu, Y. Xu, Y. Liu, C. Luo, C. Wang, *Nanoscale* **2013**, 5, 780.
52. D. Shimizu, S. Nishimura, P. Barpanda, A. Yamada, *Chem. Mater.* **2012**, *24*, 2598.
53. K. Momma, F. Izumi, *J. Appl. Crystallogr.* **2008**, *41*, 653.